

# Evaluation of the microstructure and properties of $\text{Cr}_3\text{C}_2$ powders added to Vanadis 4 alloy steel via vacuum sintering and heat treatments

S.-H. Chang<sup>1\*</sup>, K.-Y. Lee<sup>1</sup>, K.-T. Huang<sup>2</sup>, T.-H. Yang<sup>1\*\*</sup>

<sup>1</sup>*Department of Materials and Mineral Resources Engineering, National Taipei University of Technology, Taipei 10608, Taiwan, R. O. China*

<sup>2</sup>*Department of Auto-Mechanics, National Kangshan Agricultural Industrial Senior High School, Kaohsiung 82049, Taiwan, R. O. China*

Received 21 September 2018, received in revised form 20 May 2019, accepted 21 May 2019

## Abstract

In this research, different ratios (1, 3, and 5 mass%) of chromium carbide ( $\text{Cr}_3\text{C}_2$ ) powders were added to Vanadis 4 alloy steel powders. The various components of the powders underwent vacuum sintering at 1235, 1250, and 1265 °C for 1 h. The heat treatment process included quenched, sub-zero, and tempering treatment afterward. The results showed that the alloy with the addition of 5 mass%  $\text{Cr}_3\text{C}$  obtained the optimal mechanical properties after sintering at the temperature of 1250 °C for 1 h. Meanwhile, the apparent porosity decreased to 0.04 %; the transverse rupture strength (TRS) and hardness reached 1821.2 MPa and 82.4 HRA, respectively. However, the hardness declined slightly to 82.3 HRA, but the TRS substantially increased to 2085.0 MPa. The decrease in hardness could be ascribed to the release of internal stress after the tempering process. Significantly, the alloy with a series of heat treatment processes was effective in enhancing strengthening TRS of the Vanadis 4 composites.

**Key words:** chromium carbide, Vanadis 4 alloy steel, vacuum sintering, porosity, transverse rupture strength, sub-zero treatment

## 1. Introduction

The cold work tool steels are the highly alloyed type of steels in comparison with conventional standard steels, having excellent properties such as high hardness, toughness, and wear resistance and used in cutting blades, rolling planes, forming, and deep drawing applications. To meet the demand mentioned above, different compositions are essential; they are alloyed with chromium, vanadium, molybdenum, tungsten, etc. [1]. Among them, Vanadis 4 steel is a powder metallurgical (PM) high alloyed steel containing (0.4 % Mn, 8.0 % Cr, 1.5 % Mo, and 4.0 % V). Vanadis 4 has similar machining abilities and heat treatment procedures for tool steel grade AISI D2 [2, 3]. The dominant strengthening mechanisms include solid-solution strengthening and precipitation hardening by chromium and vanadium carbides, respec-

tively. Therefore, the Vanadis 4 steel offers an extremely excellent combination of wear resistance and ductility for high-performance cold work tool steels [2–4].

Also, metal matrix composites (MMCs) are widely used in many fields of engineering materials. These materials provided suggestively adjusted properties such as high strength, hardness, and stiffness in comparison to the conventional monolithic materials [5]. On the other hand, MMCs innovated to improve the mechanical wear resistance by introducing a ceramic phase (the reinforcement) in their microstructure [6]. In recent years, iron-based alloy steels have been used as matrix materials for metal-matrix composites owing to the low cost, versatility, and adequate mechanical and wear properties [7, 8]. However, several metal-ceramic compound alloys were studied, but only a few found a noteworthy commercial application: the gen-

\*Corresponding author: e-mail address: [changsh@ntut.edu.tw](mailto:changsh@ntut.edu.tw)

\*\*Corresponding author: e-mail address: [yangdavid180@gmail.com](mailto:yangdavid180@gmail.com)

eral carbides-base (NbC, VC, TiC, TaC, WC, Cr<sub>3</sub>C<sub>2</sub> additive) is used as MMCs [6–9].

To improve the properties of a novel MMCs technique, many studies have focused on the effects of grain growth inhibitors. Among them, chromium carbide (Cr<sub>3</sub>C<sub>2</sub>) is the most effective grain growth inhibitor due to its high solubility and mobility in the metal matrix phase [10–12]. The widely accepted inhibition mechanism of Cr<sub>3</sub>C<sub>2</sub> is related to its ability to slow solution/re-precipitation reactions during the liquid phase sintering (LPS) of the PM process [13–15]. PM is a smart method for fabrication of high alloy and high melting materials with excellent mechanical properties. The process of the vacuum sintering is a very important procedure to achieve the dense and ultra-fine grain structure by densifying the powder materials [16]. Moreover, LPS is well recognized as a convenient process route achieving near-full theoretical sintered densities for many PM ferrous alloys [17, 18]. However, the inhibition mechanisms for Cr<sub>3</sub>C<sub>2</sub> during LPS are still not unequivocal.

Our previous studies also indicated that heat treatment could be used to increase the strength and hardness of as-sintered PM alloy steel [3, 4, 8]. However, it is still unclear whether Vanadis 4 alloy steel with different amounts of Cr<sub>3</sub>C<sub>2</sub> particles in the strengthening phase can obtain better mechanical properties, as well as better distribution and size of the carbides for Vanadis 4 composites after heat treatment. Therefore, the present research aims to explore a series of vacuum sintering processes and heat treatments for Vanadis 4 composites, as well as to examine their effects on the microstructure, mechanical properties and corrosion behavior of Cr<sub>3</sub>C<sub>2</sub> strengthened Vanadis 4 alloy steel.

## 2. Experimental procedures

This study used Vanadis 4 alloy steel powders as a substrate and added different ratios of Cr<sub>3</sub>C<sub>2</sub> powders as a strengthening phase. To obtain more uniform Vanadis 4 powders, particle sizes smaller than  $30 \pm 1 \mu\text{m}$  were sifted from the original powders. The chemical compositions (mass%) of the Vanadis 4 alloy steel powders are as follows: 1.51 % C, 1.0 % Si, 0.4 % Mn, 8.0 % Cr, 1.5 % Mo, 4.0 % V, and 83.59 % Fe. Furthermore, the different amounts of Cr<sub>3</sub>C<sub>2</sub> powders (1, 3, and 5 mass%) were mixed and added to Vanadis 4 alloy steel powders, designated as Cr1, Cr3, and Cr5, hereafter. After milling, the PVA (polyvinyl alcohol) as a binder was added. The green compact ( $40 \times 6 \times 6 \text{ mm}^3$ ) of the powder specimen was produced under the uniaxial pressure at 300 MPa for 5 min.

To explore the effects of a series of vacuum sintering and heat treatments, the vacuum sintering temperatures were set at 1235, 1250, and 1265 °C for 1 h

in a  $5 \times 10^{-3}$  Pa. However, when the sintering temperature was increased to 1280 °C, a partly melting phenomenon appeared in the sintered specimens. Besides, heat treatment steps (quenching followed by sub-zero and tempering) were performed, in which the samples were heated to 1020 °C and the temperature was maintained for 100 min for quenching with 0.5 MPa of N<sub>2</sub> as the quenching media. The samples were subjected to sub-zero treatment at a temperature of –150 °C for 60 min. The tempering temperature was held at 480 °C for 3 h, and then cooled to room temperature, and this aging process performed twice repeatedly.

In order to evaluate the sintered behavior of Vanadis 4 alloy steels added Cr<sub>3</sub>C<sub>2</sub> powders by vacuum sintering and heat treatments, various material characterization techniques were used, including apparent porosity, mean grain size (linear intercept method), hardness, transverse rupture strength (TRS), and corrosion tests (Potential Stat Chi 601). Microstructural observations of the specimens were performed by optical microscopy (OM) and scanning electron microscopy (SEM, Hitachi-S4700). The apparent porosity measurement used the Archimedes principle, which followed the ASTM B311-08 and C830 standards. Hardness tests were performed by Rockwell A hardness (HRA, Indentec 8150LK) with a loading of 588.4 N, which followed the ASTM B294 standard. The Hung Ta universal material test machine (HT-9501A) with a maximum load of 245 kN was used for the TRS tests (ASTM B528-05). Meanwhile, the TRS was obtained by the equation  $R_{\text{bm}} = 3FLk/2bh^2$ , where  $R_{\text{bm}}$  is the TRS, which is determined as the fracture stress in the surface zone,  $F$  is the maximum fracture load. In this work,  $L$  was 30 mm,  $k$  was a chamfer correction factor (normally 1.00–1.02), and  $b$  and  $h$  were 5 mm. The specimen dimensions for the TRS test were  $5 \times 5 \times 40 \text{ mm}^3$  and tested were at least three pieces.

The corrosion potential analysis uses three electrodes method: the reference electrode is a saturated chloride solution of silver-silver chloride electrode, an auxiliary electrode is a platinum electrode, and the working electrode is connected to the test specimens (ASTM G59-97). The contact area of the specimen was  $0.785 \text{ cm}^2$ . The corrosive solvent was used 3.5 mass% NaCl solution and was maintained at room temperature. Scanning speed of  $0.01 \text{ v s}^{-1}$ , the initial potential of –2.0 V, and the final potential of 2.0 V practiced. The polarization curve was obtained by Corr-View software to analyze and compare the corrosion potential ( $E_{\text{corr}}$ ), the corrosion resistance ( $R_{\text{corr}}$ ), and corrosion current ( $I_{\text{corr}}$ ) of the different sintering parameters [3, 4]. Finally, a comparison conducted to investigate the corrosion current ( $I_{\text{corr}}$ ) and polarization resistance ( $R_{\text{p}}$ ) of the different sintered and heat-treated Vanadis 4 composites.

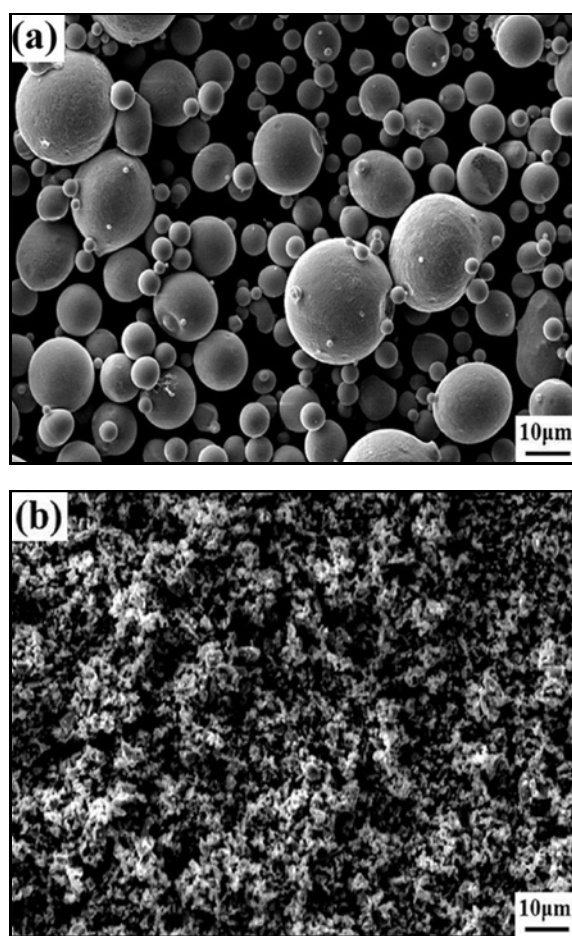


Fig. 1. The SEM images of the surface morphology of (a) the sifted Vanadis 4 alloy steel powders, (b) the original  $\text{Cr}_3\text{C}_2$  powders, and (c) Vanadis 4- $\text{Cr}_3\text{C}_2$  powders after 6 h ball mixing.

### 3. Results and discussion

This study used Vanadis 4 alloy steel powders as a substrate and added different ratios of  $\text{Cr}_3\text{C}_2$  powders as a strengthening phase. To obtain more uniform Vanadis 4 powders, particle sizes smaller than  $30 \pm 1 \mu\text{m}$  were sifted from the original powders. As a result, the distribution of the powder ranges from  $8.5 \pm 0.5$  to  $26.2 \pm 0.5 \mu\text{m}$ ; the mean particle size of the Vanadis 4 alloy steel powders was  $17.3 \pm 0.5 \mu\text{m}$ , as shown in Fig. 1a. The powders possess a uniform and spherical appearance; the surface morphology of  $\text{Cr}_3\text{C}_2$  additives is shown in Fig. 1b. The mean particle size of the  $\text{Cr}_3\text{C}_2$  powders was about  $1.5 \pm 0.5 \mu\text{m}$ ; moreover, the apparent shape of the  $\text{Cr}_3\text{C}_2$  powders presented an irregular polygon, rough or undulating surfaces. Also, the mixed powders were milled by rolling the WC balls for 6 h. Figure 1c shows the morphology under the effect of mechanical alloying by ball milling for 6 h, and the mixed alloy powders produce ominously plastic deformation. Chromium car-

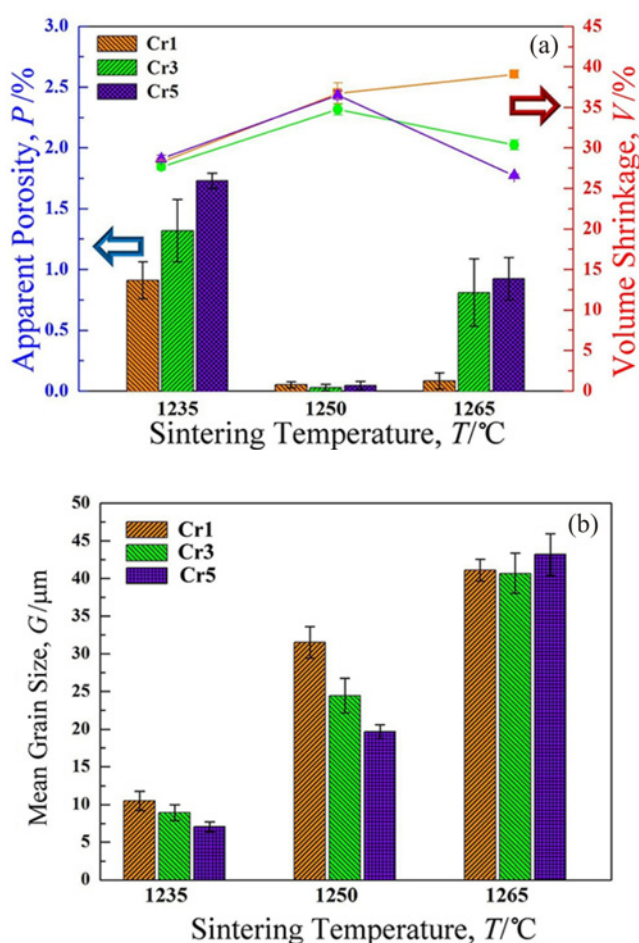


Fig. 2. Comparison of the (a) apparent porosity and volume shrinkage and (b) mean grain size of various mass%  $\text{Cr}_3\text{C}_2$  added Vanadis 4 by different sintering temperatures.

bide played a strengthening phase that was attached as a pre-alloy on the Vanadis 4 powders due to the press of the milled impact, as indicated by the arrows.

Figure 2 represents the apparent porosity, volume shrinkage, and mean grain size at different sintering temperatures when various amounts of  $\text{Cr}_3\text{C}_2$  were added to the Vanadis 4 specimens. Significantly, the apparent porosity of the Cr1, Cr3, and Cr5 specimens was higher compared with the samples without any additive after sintering at the temperature 1235°C for 1 h, as shown in Fig. 2a. In general, it has high thermal energy for extending the diffusion time by raising the temperature for supporting the sintering process. When the sintering temperature increased to 1250°C, the apparent porosity decreased rapidly. The porosity levels of the Cr1, Cr3, and Cr5 specimens were 0.05, 0.03, and 0.04%, respectively. It was reasonable to prove that all the specimens owned a sufficient diffusion time without evidence of pores. However, when the sintering temperature was further increased to

1265 °C, the apparent porosity of the Cr3 and Cr5 specimens occurred upward tendency, with porosity level values of 0.81 and 0.92 %, respectively; it should be relative to the Ostwald ripening phenomenon during a high-temperature sintering process [3]. As a result, the apparent porosity level of the alloy with high Cr content indicated an apparent increase, especially sintered at too high sintering temperature.

In this work, the volume shrinkage of the Cr1, Cr3, and Cr5 specimens showed a similar trend regarding apparent porosity, as shown in Fig. 2a. When the sintering temperature approached to 1235 °C, all the specimens had relatively low volume shrinkage resulting from the restricted diffusion capability owing to the  $\text{Cr}_3\text{C}_2$  barrier. The thermal driving force was not sufficient for the diffusion behavior when the sintering temperature was not high enough at 1235 °C. When the sintering temperature increased to 1250 °C, the volume shrinkage of all the specimens showed a significant increase. Among them, the volume shrinkage of 28.2, 27.7, and 28.7 % for the Cr1, Cr3, and Cr5 specimens increased to 36.7, 34.7, and 36.5 %, respectively. When the sintering temperature further increased to 1265 °C, the volume shrinkage of the Cr1 specimens represented a slowly increasing trend (39.1 %). However, the Cr3 and Cr5 specimens showed a decreasing phenomenon (30.4 and 26.6 %, respectively) due to a high-temperature causing local liquid phase sintering (LPS) occurrence. It was reasonable to speculate that it was easier for a small amount of added  $\text{Cr}_3\text{C}_2$  powders to be rearranged and filled the interspaces of the Vanadis 4 particles during the sintering process.

Also, an excess of  $\text{Cr}_3\text{C}_2$  powders, such as Cr3 and Cr5, easily obstructed the extension of the liquid phase during the sintering process. The porosity level (1.32 and 1.73 %) of the specimens increased with the amount of  $\text{Cr}_3\text{C}_2$  powders (3 and 5 %) after vacuum sintering temperature 1235 °C for 1 h as a result of incomplete liquid phase sintering. An optimal sintering parameter was not found due to the higher apparent porosity remains in the specimens after sintering at the temperature 1235 °C for 1 h. However, the porosity level of all the specimens dramatically decreased to less than 1 % when vacuum sintering raised the temperature to 1250 °C for 1 h. It was possible that a sintering temperature of 1250 °C corresponded to the appropriate LPS temperature for the sintered Cr1, Cr3, and Cr5 specimens, hence an appropriate density of the sintering materials was obtained by controlling the amount of additive chromium carbide and sintering temperature of 1250 °C.

Figure 2b shows the mean grain size at different sintering temperatures for various amounts of  $\text{Cr}_3\text{C}_2$  added to the Vanadis 4 specimens. The mean grain sizes of the Cr1, Cr3, and Cr5 specimens were 10.52, 8.92, and 7.04  $\mu\text{m}$  after sintering at 1235 °C for 1 h, respectively. Furthermore, the mean grain sizes for the

Cr1, Cr3, and Cr5 specimens showed a substantial increase to 31.54, 24.47, and 19.68  $\mu\text{m}$  after sintering at 1250 °C for 1 h, respectively, while the values for the Cr1, Cr3, and Cr5 specimens after sintering at 1265 °C for 1 h were 41.12, 40.69, and 43.20  $\mu\text{m}$ , respectively. It is worth noting that the mean grain size revealed a significant decreasing trend as the added amounts of  $\text{Cr}_3\text{C}_2$  increased, but the mean grain size also showed obvious grain growth as the sintering temperature increased. Therefore, it is reasonable to speculate that the  $\text{Cr}_3\text{C}_2$  additives are effective in inhibiting grain growth in Vanadis 4 alloy steel. These results will be verified in subsequent microstructure observations.

Figure 3 reveals the OM images of the Cr1, Cr3, and Cr5 specimens after sintering at 1235 °C for 1 h. As seen in Figs. 3a–c, the amount and size of the residual porosity increased as the added amounts of  $\text{Cr}_3\text{C}_2$  increased. Meanwhile, the clusters of MC carbides precipitated on the grain boundaries, and these increased as the added amount of  $\text{Cr}_3\text{C}_2$  additive increased. So, the more  $\text{Cr}_3\text{C}_2$  additive was added, the higher the sintering driving force was required for the similar diffusion potential. If the sintering temperature were not high enough, it would lead to the liquid phase not fill the porosities sufficiently, causing increased extra pores. Therefore, it can be deduced that the sintering temperature of 1235 °C was insufficient for the Cr1, Cr3, and Cr5 specimens to diffuse for enhancing the sintering densification.

When the sintering temperature increased to 1250 °C, the OM images of the Cr1, Cr3, and Cr5 specimens illustrated more distinct microstructures, as shown in Fig. 4. Only a few pores persist within the matrices after sintering at 1250 °C for 1 h, as shown in Figs. 4a–c. The number of pores showed an obvious decrease after sintering at 1250 °C for 1 h compared to that sintered at 1235 °C (Fig. 3). Moreover, increasing the added amount of  $\text{Cr}_3\text{C}_2$  powders resulted in a momentous decrease in the mean grain size (31.54  $\rightarrow$  24.47  $\rightarrow$  19.68  $\mu\text{m}$ ). The Cr5 specimen possessed the smallest grain sizes after sintering at 1250 °C for 1 h, as shown in Fig. 4c. The result confirmed that increasing the added amount of  $\text{Cr}_3\text{C}_2$  powder inhibited grain growth. In other words,  $\text{Cr}_3\text{C}_2$  powders played an important role in inhibiting grain growth during the sintering process.

Additionally, since the content of  $\text{Cr}_3\text{C}_2$  additive was less, the carbides of the Cr1 specimens dispersed in the grain boundaries were less than those of the Cr3 and Cr5 specimens. Conversely, the precipitated carbides in the grains were dramatically more numerous than those in the Cr3 and Cr5 specimens. Moreover, the precipitated carbides in the grains and on the grain boundaries (the gray particles) were predominantly vanadium, which would be supported by the subsequent quantitative analysis using EDS. As previously noted, the principal strengthening mecha-

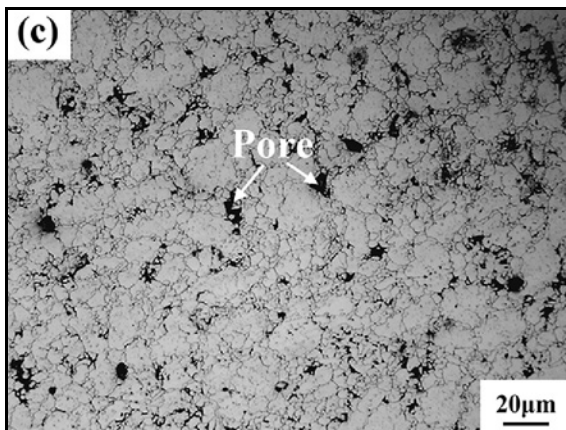
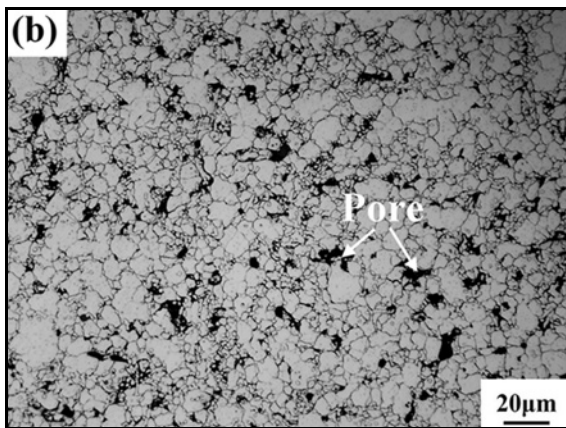
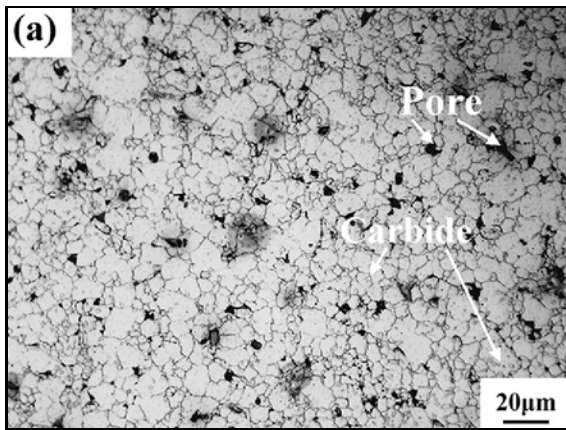


Fig. 3. The OM images of various mass%  $\text{Cr}_3\text{C}_2$  added Vanadis 4 after sintering at  $1235^\circ\text{C}/1\text{ h}$ : (a) Cr1, (b) Cr3, and (c) Cr5.

nisms of Vanadis 4 composites included solid-solution strengthening and precipitation hardening by vanadium and chromium carbides, respectively. As seen in Fig. 4c, the plate-shaped carbides ((Cr, V) carbides) in the grain boundaries appear. Besides, the precipitated carbides of the Cr5 specimen on the grain boundaries were quite uniform and widespread, and the size of the carbides was also relatively small. Simultaneously, the amount of precipitated carbides within the grains

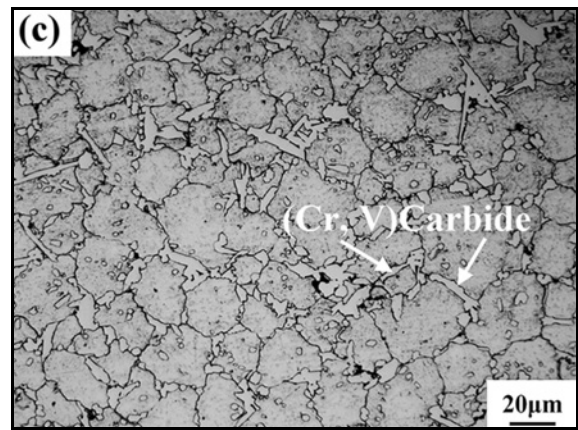
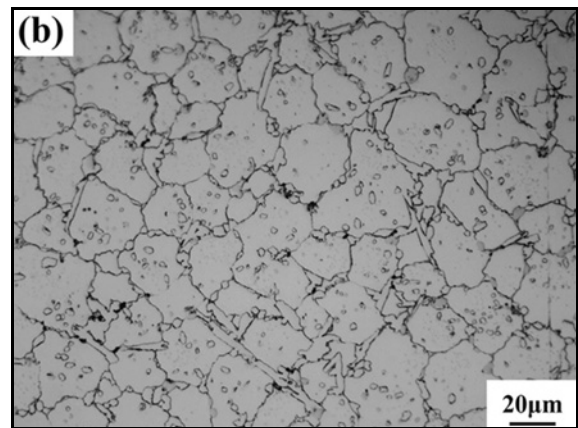
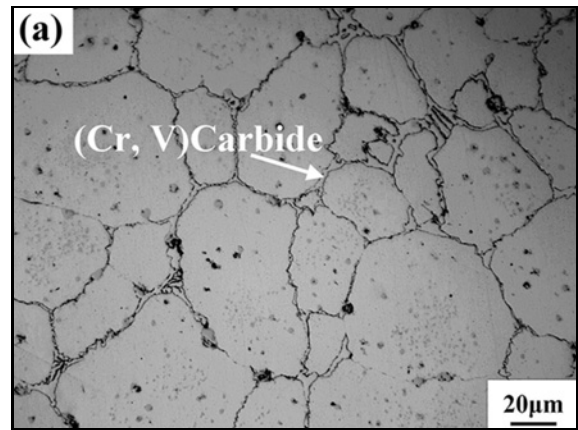


Fig. 4. The OM images of various mass%  $\text{Cr}_3\text{C}_2$  added Vanadis 4 after sintering at  $1250^\circ\text{C}/1\text{ h}$ : (a) Cr1, (b) Cr3, and (c) Cr5.

was considerably less than that of Cr1 and Cr3. It was reasonable to suggest that the optimal mechanical properties would be obtained after a suitable sintering temperature ( $1250^\circ\text{C}$ ). This argument can be verified in the subsequent experiments.

Figure 5 shows the OM images of the Cr1, Cr3, and Cr5 specimens after sintering at the temperature of  $1265^\circ\text{C}$  for 1 h. As further compared with Fig. 4, all of the specimens represented that the mean

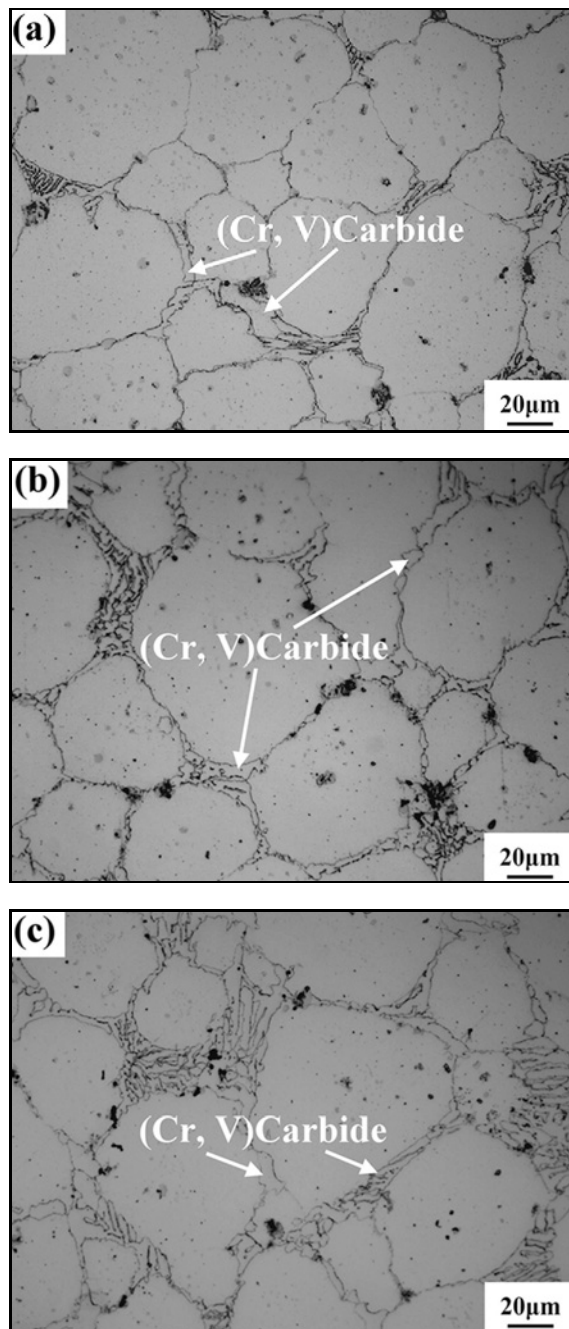


Fig. 5. The OM images of various mass%  $\text{Cr}_3\text{C}_2$  added Vanadis 4 after sintering at  $1265^\circ\text{C}/1\text{ h}$ : (a) Cr1, (b) Cr3, and (c) Cr5.

grain size increased after sintering at the temperature of  $1265^\circ\text{C}$ . In general, the high sintering temperature easily caused a grain-coarsening phenomenon and rapid growth of carbides. In the research, an evident grain-coarsening phenomenon appeared in the  $1265^\circ\text{C}$ -sintered specimens. Furthermore, the plate-shaped carbides ((Cr, V) carbides) still appeared in the grain boundaries, which resulted in the inhibited effects of carbide precipitation and grain-

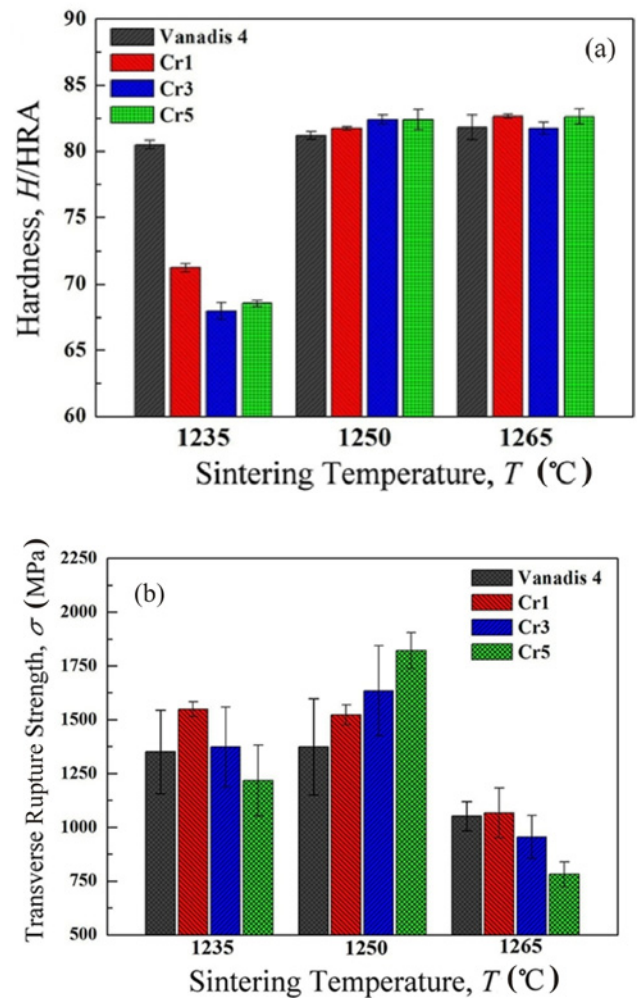


Fig. 6. Comparison of the hardness and TRS of various mass%  $\text{Cr}_3\text{C}_2$  added Vanadis 4 by the different sintering temperatures: (a) hardness and (b) TRS.

coarsening. Nevertheless, the gray precipitates on the grain boundaries of Cr3 are mainly  $\text{M}_7\text{C}_3$  carbides, as indicated by the arrows. Also, all of the Vanadis 4 composite specimens with  $\text{Cr}_3\text{C}_2$  added nearly melted after sintering at  $1280^\circ\text{C}$  for 1 h, which rendered the specimens unfit for subsequent research and testing. According to the above discussion and results, the optimal vacuum sintering temperature for  $\text{Cr}_3\text{C}_2$  added to Vanadis 4 alloy steel should be  $1250^\circ\text{C}$ .

Figure 6 shows the hardness and TRS test results of the Vanadis 4, Cr1, Cr3, and Cr5 specimens after the different sintering temperatures. All of the experimental values for hardness and TRS are shown in Tables 1, 2. The hardness of the Cr1, Cr3, and Cr5 specimens was relatively low when the sintering temperature was of  $1235^\circ\text{C}$  for 1 h (as seen in Fig. 6a), which indicates that the specimens did not reach a complete LPS. However, the Vanadis 4 specimens (no  $\text{Cr}_3\text{C}_2$  added) had a moderately high hardness value

Table 1. Comparison of the hardness (HRA) of various mass% Cr<sub>3</sub>C<sub>2</sub> added Vanadis 4 after different sintering temperatures and heat treatments

Sintering temperature (°C)	Vanadis 4	Cr1	Cr3	Cr5	Cr5 + HT	Cr5 + SZ
1235	80.5	71.2	67.9	68.6	–	–
1250	81.2	81.7	82.4	82.4	81.3	82.3
1265	81.8	82.7	81.7	82.6	–	–

Table 2. Comparison of the TRS value (MPa) of various mass% Cr<sub>3</sub>C<sub>2</sub> added Vanadis 4 after the different sintering temperatures and heat treatments

Sintering temperature (°C)	Vanadis 4	Cr1	Cr3	Cr5	Cr5 + HT	Cr5 + SZ
1235	1350.9	1549.2	1373.2	1217.3	–	–
1250	1370.6	1521.9	1634.4	1821.2	1921.5	2085.0
1265	1051.6	1067.1	954.2	780.9	–	–

(80.5 HRA). It indicates that the composites with the addition of Cr<sub>3</sub>C<sub>2</sub> carbides required a higher sintering temperature for achieving a condition of full densification. As the sintering temperature increased to 1250°C, the apparent porosity decreased rapidly, as shown in Fig. 2a. Therefore, the hardness of the Vanadis 4, Cr1, Cr3, and Cr5 specimens was noticeably enhanced (hardness values were 81.2, 81.7, 82.4, and 82.4 HRA, respectively). The hardness values further improved when the sintering temperature raised to 1265°C. Only the Cr3 specimen showed a slight downward tendency, but the difference is insignificant. Meanwhile, the hardness values of the Vanadis 4, Cr1, Cr3, and Cr5 specimens were 81.8, 82.7, 81.7, and 82.6 HRA, respectively.

Figure 6a also shows that the hardness value increased apparently between 1235°C and 1250°C sintering. Consequently, all of the 1250°C-sintered specimens transformed as a complete LPS, possessing appropriate hardness. Under the sintering temperature of 1250°C, all the hardness values of Cr1, Cr3, and Cr5 were higher than those of the Vanadis 4 alloy steel. Besides, the hardness values of the specimens improved slightly when the added amount of Cr<sub>3</sub>C<sub>2</sub> powder increased. As a result, it was reasonable to suggest that suitably reinforced Cr<sub>3</sub>C<sub>2</sub> powders added to the Vanadis 4 alloy steel matrix effectively enhanced the hardness.

Figure 6b represents the TRS test results for the Vanadis 4, Cr1, Cr3, and Cr5 specimens at different sintering temperatures. As the sintering temperature increased (1235 → 1250 → 1265°C), most of the TRS values increased, and then declined afterward. Almost all specimens had higher TRS values after sintering at the temperature 1250°C for 1 h; the Cr5 specimen possessed the highest TRS value (1821.2 MPa). Our previous studies showed precipitated carbides and porosity levels of Vanadis 4 composite materials acted as the important factors directly to impact the TRS value [3,

8, 9]. The results can be further compared with those of the Vanadis 4 specimen. As shown in Fig. 6b, the TRS value of the Cr5 specimen dramatically improved after sintering at 1250°C for 1 h. However, the high-temperature sintering (1265°C) that caused a significant grain-coarsening phenomenon (Fig. 5) seemed to be related to the TRS values of the Cr1, Cr3, and Cr5 specimens. Nevertheless, the Cr<sub>3</sub>C<sub>2</sub> added to Vanadis 4 alloy steels exhibited obstructed grain growth effects. This result conforms to the OM image observation, as shown in Figs. 3–5.

Also, Fig. 2a shows that the Cr3 and Cr5 specimens had a slightly higher porosity level (0.81 and 0.92%) after sintering at the temperature 1265°C for 1 h. The high porosity is undesirable to the TRS performance causing the decrease of the TRS values of Cr3 and Cr5 rapidly (954.2 and 780.9 MPa), as shown in Table 2. Notably, all of the hardness and TRS values of the Vanadis 4, Cr1, Cr3, and Cr5 specimens increased after sintering at the temperature 1250°C for 1 h. A further comparison with Vanadis 4 shows that the hardness and TRS values of the composites with the addition of Cr<sub>3</sub>C<sub>2</sub> powders meaningfully improved. Among them, the TRS values of Vanadis 4 and 1250°C-sintered Cr5 specimens were 1370.6 and 1821.2 MPa, respectively. As a result, added 5 mass% Cr<sub>3</sub>C<sub>2</sub> to Vanadis 4 alloy steel after sintering at 1250°C for 1 h increased the hardness (81.2 to 82.4 HRA) and TRS (1370.6 to 1821.2 MPa) value by 1.5 and 24.7%, respectively. It is reasonable to conclude that adding a suitable amount of carbides to Vanadis 4 alloy steel effectively decreased the porosity (0.03%) and enhanced the hardness, especially in the performance of the TRS tests.

Figure 7 shows the fracture features of the Cr1, Cr3, and Cr5 specimens after sintering at the temperature of 1250°C for 1 h. The Cr1 specimens exhibited the observable cleavage fractures with river pattern morphology after the TRS tests, as shown in

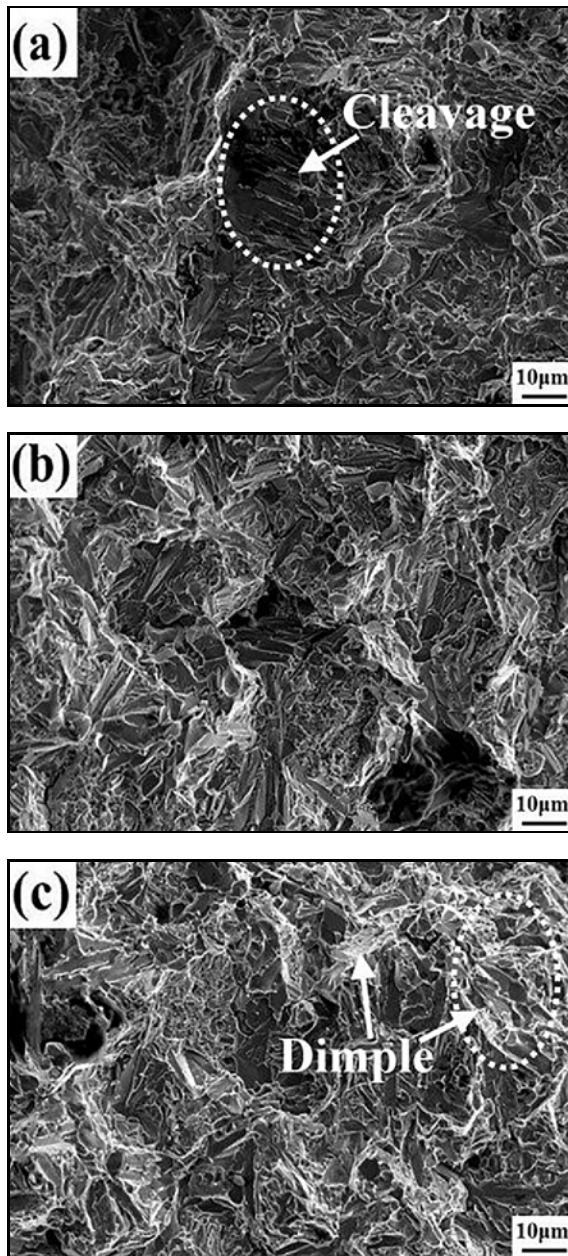


Fig. 7. The fracture surfaces of various mass%  $\text{Cr}_3\text{C}_2$  added Vanadis 4 after sintering at  $1250^\circ\text{C}/1\text{ h}$ : (a) Cr1, (b) Cr3, and (c) Cr5.

Fig. 7a. Although the fractural surface existed with a few smooth and planar brittle cleavages, it was accompanied with some rough ductile dimple fractures around the rim contour profile of the brittle cleavage to form a complex rose fractural pattern in the Cr3 specimens, as shown in Fig. 7b. Meanwhile, the cleavage fractures showed a decreasing tendency with the content of Cr concentration, and some dimple pattern acted on the edge of the cleavage surface. In contrast, the Cr5 specimens have a large number of dimple fractures after TRS tests, as shown in Fig. 7c. The mor-

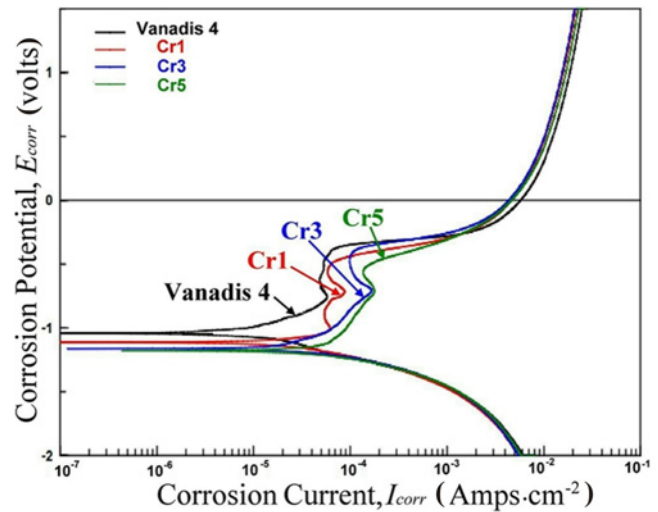


Fig. 8. Tafel results of  $1250^\circ\text{C}$ -sintered Vanadis 4,  $1250^\circ\text{C}$ -sintered Cr1, Cr3, and Cr5 specimens after 3.5 mass% NaCl corrosion tests.

phology of the fractural cross-sectional fractography is consistent with the TRS values shown in Fig. 6b.

Generally speaking, when the amount of the deformation exceeds its upper limit of the elastic deformation, the crack nucleates, grows and propagates directly under the situation of the concentrated stress, which is detrimental to the fracture resistance of the interface [3]. The general aspect of the fracture showed dimpled ruptures and small carbides cleavages. In this work, the  $\text{Cr}_3\text{C}_2$  performed as hard and brittle reinforced carbides in the grain boundaries that contributed to the fractural mechanisms of brittleness to quasi-cleavage. Moreover, the dimple fracture produced from the Vanadis 4 alloy steel itself and the influence of the metallic carbides as a barrier that can collect the concentrated stress to donate the moveable dislocation led to piling up of the dislocation as the origin of its ductility propagation. The cross-sectional fractography was in agreement with the definition that small cleavages more easily generated on the grain boundaries.

Figure 8 reveals the Tafel slope results of  $1250^\circ\text{C}$ -sintered Vanadis 4, Cr1, Cr3, and Cr5 after the 3.5 mass% NaCl corrosion test. All of the specimens exhibited a significant passivation phenomenon, i.e., the passivation surface possessed a protective purpose, especially the Vanadis 4 specimens. In other words, it showed that the sintered Vanadis 4 had excellent corrosion resistance. All the experimental data for the corrosion tests are shown in Table 3. The corrosion resistance of the Vanadis 4 composites decreases gradually with the increase of  $\text{Cr}_3\text{C}_2$  content owing to the occurrence of intergranular corrosion. It was possible that with the increased carbide content, the activity of grain boundaries could be excited increasingly. As a

Table 3. Comparison of the corrosion resistance of 1250°C-sintered Vanadis 4, 1250°C-sintered Cr1, Cr3 and Cr5 specimens after 3.5 mass% NaCl corrosion tests

	V4	Cr1	Cr3	Cr5
$I_{\text{corr}} (\times 10^{-4} \text{ A cm}^{-2})$	61.2	1.5	4.3	4.5
$E_{\text{corr}} (\times 10^{-1} \text{ V})$	-1.40	-1.40	-1.12	-0.98
$R_{\text{p}} (\times 10^3 \text{ } \Omega \text{ cm}^2)$	2.19	1.35	1.31	0.74

Table 4. The EDS analysis of the Figs. 9a,b

Elements (at.%)	(a)-1	(a)-2	(b)-1	(b)-2
C	54.06	40.33	51.27	14.16
V	3.66	5.38	8.36	8.66
Cr	42.28	25.06	21.61	31.93
Fe	–	29.23	18.76	45.25

result, the chromium carbide precipitated at the grain boundaries and thus reduced corrosion resistance. In this study, the increased amount of  $\text{Cr}_3\text{C}_2$  led to increasing significant corrosion current ( $1.5 \rightarrow 4.3 \rightarrow 4.5 \times 10^{-4} \text{ A cm}^{-2}$ ). Meanwhile, the polarization resistance indicated a declining tendency ( $1.35 \rightarrow 1.31 \rightarrow 0.74 \text{ } \Omega \text{ cm}^2$ ). Although the Cr1 specimen possessed the minimum corrosion current and maximum polarization resistance, the difference of the corrosion currents for all specimens was insignificant. Consequently, the Cr5 specimen not only possessed the high hardness and high strength but also owned an adaptable corrosion resistance. Besides, Fig. 8 also exhibits that the Cr5 specimen possesses a significant passivation curve. According to the above discussion and results, it was reasonable to say that the Cr5 specimen had good corrosion resistance, optimal microstructure, and mechanical properties after sintering at 1250°C for 1 h.

Figure 9a presents the SEM images of the Cr5 specimen sintered at 1250°C. Our previous studies indicated that the plate-shaped carbides in the grain boundaries and spherical-shaped carbides within the grains usually were  $\text{M}_7\text{C}_3$  and MC carbides, respectively [3, 8]. In this work, the EDS analysis showed that the plate-shaped carbides (Location 1) in the grain boundaries had a high content of Cr-rich (42.28 at.% Cr), as listed in Table 4 ((a)-1). It was reasonable to surmise that these plate-shaped carbides belonged to Cr-rich  $\text{M}_7\text{C}_3$  carbides. Besides, a few refined and spherical-shaped carbides within the grains (Location 2) were observed. The EDS analysis results also presented that these carbides within the grains possessed a high content of Cr-rich and Fe-rich (25.06 at.% Cr and 29.23 at.% Fe, respectively), as listed in Table 4 ((a)-2); the composition of the refined and spherical-shaped carbides was analyzed as the Cr-rich phases and Fe-rich  $\text{M}_{23}\text{C}_6$  carbides.

Figure 9b shows the SEM images of the 1250°C-

-sintered Cr5 specimens after heat treatment (Cr5 + HT). The EDS analysis represents that the plate-shaped carbides transform into the rod-shaped (Location 1) carbides, which appear in the grain boundaries to be the Cr-rich and Fe-rich (21.61 at.% Cr and 18.76 at.% Fe, respectively), as listed in Table 4 ((b)-1). As previously noted, the rod-shaped carbides were identified as the Cr-rich phases and Fe-rich  $\text{M}_{23}\text{C}_6$  carbides. On the other hand, a larger number of the spherical-shaped carbides within the grains (Location 2) with a higher Cr and Fe content (31.93 at.% Cr and 45.25 at.% Fe, respectively), as listed in Table 4 ((b)-2), indicates the presence of (Fe, Cr) and  $\text{Fe}_3\text{C}$  carbides, respectively, which is consistent with our previous studies [3, 8]. Figure 9c shows the SEM images of the 1250°C-sintered Cr5 specimens after the post-heated treatment of the quenching, sub-zero, and tempering processes (Cr5 + SZ). The (Fe, Cr) carbides appeared within the grains, while  $\text{M}_{23}\text{C}_6$  carbides produced on the grain boundaries after the quenching, sub-zero and tempering treatments. This result of the observation is consistent with Fig. 9b. Notably, it is found that Fig. 9c displays the smaller particle size of the carbide precipitation in the grains as compared with Fig. 9b. It could improve its mechanical properties due to the smaller-sized carbides precipitated in progress.

A further comparison was made of the different treatments of Vanadis 4 alloy steel with the different content of the Cr carbides additives for enhancing the mechanical properties. As seen in Table 1, the hardness value of 1250°C-sintered Vanadis 4 is 81.2 HRA, whereas the hardness values of Cr5 (sintered), Cr5 + HT (the quenched and tempering) and Cr5 + SZ (the quenched, sub-zero and tempering) are 82.4, 81.3, and 82.3 HRA, respectively. The high hardness value of the sintered Cr5 sample performed owing to the existence of the  $\alpha'$ -martensitic phases by XRD analysis. Moreover, the solid solutions strengthening of the

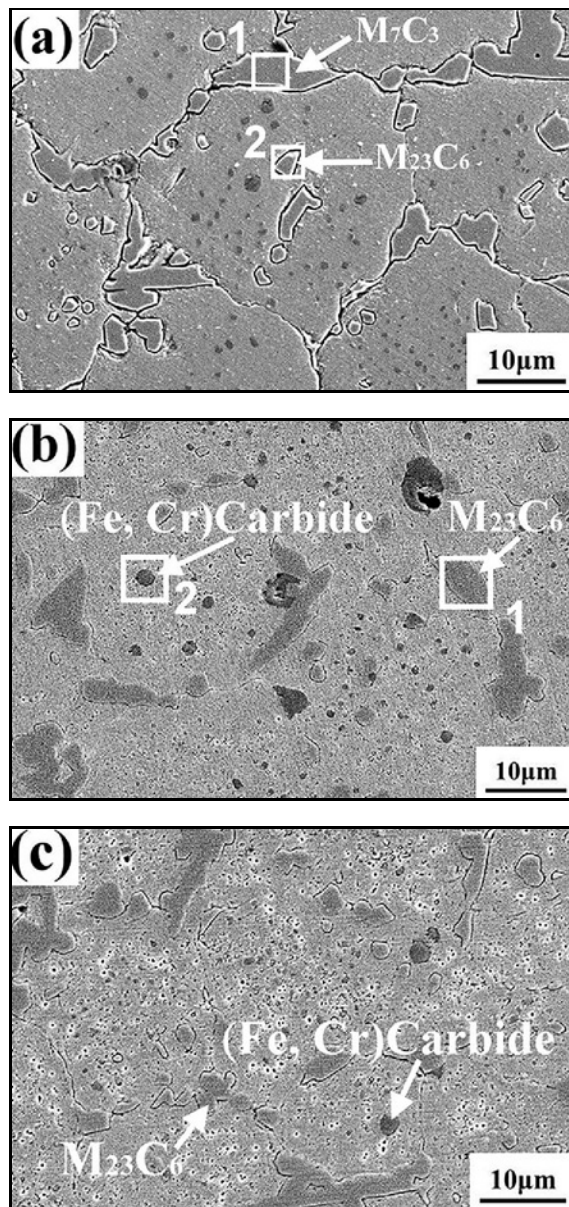


Fig. 9. The SEM images of the optimal sintered-Cr5, Cr5 + HT and Cr5 + SZ specimens: (a) Cr5, (b) Cr5 + HT, and (c) Cr5 + SZ.

alloys were accompanied by occurring in the martensitic and austenitic phases. The sintered Cr5 specimen did not transfer to a fully tempered martensitic microstructure from the  $\gamma$ -austenite phase and still had a residual remaining of the  $\gamma$ -austenite phase. Previous studies indicated that sub-zero treatment could encourage the phase transformation of carbide formation during tempering, leading to increased hardness [1, 3]. Besides, our previous study also confirmed that in the sub-zero and post-heated treatments, the variation in hardness was dominated by the tempering process, which released the internal stress from the tempering treatment and resulted in decreasing the

hardness value [3]. As a result, the hardness values of Cr5 + HT and Cr5 + SZ specimens were slightly lower than those of Cr5, but the hardness values of the alloys with Cr additives by the post-heated treatment were higher than those of the Vanadis 4 without any additional carbides.

Our previous study showed that the optimization of the condition of the heat treatment effectively adjusted the size of the carbide particle in the alloy steel composite, but did not arrange the distribution of the carbide particles [3, 4, 8]. An excess amount of carbide additive made the heterogeneous precipitation of the carbide compound to accumulate and assemble in the grain boundaries after sintering, which was detrimental to the TRS values. In the present work, the TRS value of the Cr5 + SZ specimen showed a significant increase, as listed in Table 2. The TRS value soared to 2085.0 MPa. As mentioned previously, the Cr5 + SZ possessed the dispersive smaller carbides uniformly and homogeneously distributed in the grains. It was reasonable to conclude that the small rod-shaped  $M_{23}C_6$  carbides in the grain boundaries and the refined (Fe, Cr) and  $Fe_3C$  carbides reprecipitated within the grains resulted in the increased TRS value. According to the above discussion and results, the Cr5 specimen sintered at the temperature 1250 °C for 1 h, followed by quenching, sub-zero, and tempering treatment, owned optimal microstructures and mechanical properties in progress [4].

#### 4. Conclusions

In this work, adding the appropriate amount of chromium carbide was effective in enhancing the mechanical properties of Vanadis 4 alloy steel after different heat treatment processes. Moreover, the  $Cr_3C_2$  additives were helpful in inhibiting grain growth. Among them, the Cr5 specimen (adding 5%  $Cr_3C_2$  powders) possessed the highest hardness (82.4 HRA) and TRS value (1821.2 MPa) after sintering at 1250 °C for 1 h. The amount of  $Cr_3C_2$  content in the alloy increased led to reducing the corrosion resistance of Vanadis 4 composites. Although the corrosion current of Cr5 specimens slightly increased, the Cr5 specimen exhibited a significant passivation phenomenon, indicating that it still owned the excellent corrosion resistance.

The plate-shaped  $M_7C_3$  carbides produced on the grain boundaries and the spherical-shaped  $M_{23}C_6$  carbides precipitated within the grains after 1250 °C-sintered Vanadis 4 specimens. Also, the 1250 °C-sintered Cr5 specimens underwent a series of quenching, sub-zero, and tempering treatments. The result revealed that the refined (Fe, Cr) carbides homogeneously precipitated within the grains, while  $M_{23}C_6$  carbides generated on the grain boundaries, which was effectively relative to the TRS value of the Cr5

composite materials. Significantly, the highest TRS (2085.0 MPa) and suitable hardness (82.3 HRA) were acquired by adding 5% Cr<sub>3</sub>C<sub>2</sub> to Vanadis 4 alloy steel after sintering at 1250°C for 1 h, followed by the quenching, sub-zero, and tempering thermal treatments in progress.

### Acknowledgements

This research was supported by the Ministry of Science and Technology of the Republic of China under Grant No. MOST 106-2221-E-027-035-. The authors would like to express their appreciations for VOESTALPINE HIGH-PERFORMANCE METALS PACIFIC PTE. LTD and ASSAB STEELS TAIWAN CO., LTD.

### References

- [1] Arslan, F. K., Altinsoy, I., Hatman, A., Ipek, M., Zeytin, S., Bindal, C.: *Vacuum*, 86, 2011, p. 370. [doi:10.1016/j.vacuum.2011.07.066](https://doi.org/10.1016/j.vacuum.2011.07.066)
- [2] Yan, F., Xu, Z., Shi, H. S., Fan, J. F.: *Mater. Charact.*, 59, 2008, p. 592. [doi:10.1016/j.matchar.2007.04.019](https://doi.org/10.1016/j.matchar.2007.04.019)
- [3] Chang, S. H., Yeh, P. T., Huang, K. T.: *Vacuum*, 142, 2017, p. 123. [doi:10.1016/j.vacuum.2017.05.015](https://doi.org/10.1016/j.vacuum.2017.05.015)
- [4] Huang, K. T., Chang, S. H., Yeh, P. T.: *ISIJ Int.*, 57, 2017, p. 1252. [doi:10.2355/isijinternational.ISIJINT-2017-033](https://doi.org/10.2355/isijinternational.ISIJINT-2017-033)
- [5] Jarzabek, D. M., Chmielewski, M., Wojciechowski, T.: *Composites: Part A*, 76, 2015, p. 124. [doi:10.1016/j.compositesa.2015.05.025](https://doi.org/10.1016/j.compositesa.2015.05.025)
- [6] Verdi, D., Garrido, M. A., Múnez, C. J., Poza, P.: *J. Alloy. Compd.*, 695, 2017, p. 2696. [doi:10.1016/j.jallcom.2016.11.185](https://doi.org/10.1016/j.jallcom.2016.11.185)
- [7] Lin, C. M.: *Vacuum*, 121, 2015, p. 96. [doi:10.1016/j.vacuum.2015.07.023](https://doi.org/10.1016/j.vacuum.2015.07.023)
- [8] Huang, K. T., Chang, S. H., Hsieh, P. C.: *J. Alloy. Compd.*, 712, 2017, p. 760. [doi:10.1016/j.jallcom.2017.04.125](https://doi.org/10.1016/j.jallcom.2017.04.125)
- [9] Chang, S. H., Tang, T. P., Huang, K. T., Tai, F. C.: *Powder Metall.*, 54, 2011, p. 507. [doi:10.1179/003258910X12740974839503](https://doi.org/10.1179/003258910X12740974839503)
- [10] Ouyang, C. X., Zhu, S. G., Dong, W. W., Qu, H. X.: *Int. J. Refract. Met. H*, 41, 2013, p. 41. [doi:10.1016/j.ijrmhm.2013.01.015](https://doi.org/10.1016/j.ijrmhm.2013.01.015)
- [11] Wu, C. C., Chang, S. H., Tang, T. P., Peng, K. Y., Chang, W. C.: *J. Alloy. Compd.*, 686, 2016, p. 810. [doi:10.1016/j.jallcom.2016.06.221](https://doi.org/10.1016/j.jallcom.2016.06.221)
- [12] Zheng, D. H., Lin, X. Q., Li, Y. Y., Qu, S. G., Yang, C.: *Ceram. Int.*, 40, 2014, p. 2011. [doi:10.1016/j.ceramint.2013.07.111](https://doi.org/10.1016/j.ceramint.2013.07.111)
- [13] Ouyang, C. X., Zhu, S. G., Qu, H. X.: *Mater. Des.*, 40, 2012, p. 550. [doi:10.1016/j.matdes.2012.04.030](https://doi.org/10.1016/j.matdes.2012.04.030)
- [14] Hussainova, I., Pirso, J., Antonov, M., Juhani, K., Letunovits, S.: *Wear*, 263, 2007, p. 905. [doi:10.1016/j.wear.2006.12.027](https://doi.org/10.1016/j.wear.2006.12.027)
- [15] Huang, S. G., Li, L., Van der Biest, O., Vleugels, J.: *J. Alloy. Compd.*, 464, 2008, p. 205. [doi:10.1016/j.jallcom.2007.10.038](https://doi.org/10.1016/j.jallcom.2007.10.038)
- [16] Chang, S. H., Chang, M. H., Huang, K. T.: *J. Alloy. Compd.*, 649, 2015, p. 89. [doi:10.1016/j.jallcom.2015.07.119](https://doi.org/10.1016/j.jallcom.2015.07.119)
- [17] Huang, K. T., Chang, S. H., Wu, M. W., Wang, C. K.: *ISIJ Int.*, 56, 2016, p. 335. [doi:10.2355/isijinternational.ISIJINT-2015-469](https://doi.org/10.2355/isijinternational.ISIJINT-2015-469)
- [18] Wang, H. T., Webb, T., Bilster, J. W.: *Int. J. Refract. Met. H*, 53, 2015, p. 117. [doi:10.1016/j.ijrmhm.2015.07.004](https://doi.org/10.1016/j.ijrmhm.2015.07.004)